Simulative study on integrated optical multimode waveguides with guided beams based on the system standardization of elements

Article · December 2022

3 authors:

Ahmed Nabih Zaki Rashed
faculty of electronic engineering menoufia university

Hasane Ahammad Shaik
K L University

Md. Amzad Hossain
Ruhr-Universität Bochum

Ahmed Nabih Zaki Rashed*, Kausar Jahan, Ali Baig Mohammad, Shaik Hasane Ahammad, Md. Amzad Hossain* and Farid Anwar Fawzy

Simulative study on integrated optical multimode waveguides with guided beams based on the system standardization of elements

https://doi.org/10.1515/joc-2022-0251
Received September 24, 2022; accepted December 10, 2022; published online December 30, 2022

Abstract: This study has outlined simulative study on integrated optical multimode waveguides with guided beams based on the system standardization of elements. Deflection of a cantilever are clarified with a point force at the free end, due to the distributed weight at the beam, with a mass at the free end, and at the free end under acceleration. The bending of a double clamped beam under its distributed weight, deflection with the central mass double clamped beam under its weight, the buckling of a double clamped beam due to a compressive stress, out of plane deflection (OPD) of a bent beam suspension, OPD of a folded beam suspension, and OPD of a serpentine beam suspension are also clarified and reviewed. Dependence of cross section of beam on torsion constant is outlined. The stiffness ratio of lateral to vertical motion of hammock suspension is also clarified. The design of a crab-leg suspension and the dependence of the stiffness on thigh section of the crab leg flexure and the design of a folded flexure suspension and the dependence of stiffness on ratio of column beam lengths are also reported.

Keywords: beam deflection; guided beams; MEMSolver simulation; stiffness ratio; surface structure.

***Corresponding authors: Ahmed Nabih Zaki Rashed**, Electronics and Electrical Communications Engineering Department Faculty of Electronic Engineering, Menoufia University, Menouf 32951, Egypt, E-mail: ahmed_733@yahoo.com. https://orcid.org/0000-0002-5338-1623; and **Md. Amzad Hossain**, Institute of Theoretical Electrical Engineering, Faculty of Electrical Engineering and Information Technology, Ruhr University Bochum, 44801 Bochum, Germany; and Department of Electrical and Electronic Engineering, Jashore University of Science and Technology, Jashore 7408, Bangladesh, E-mail: mahossain.eee@gmail.com
Kausar Jahan, Department of ECE, Dadi Institute of Engineering and Technology, Anakapalle, Andhra Pradesh, India, E-mail: kjahan@diet.edu.in
Ali Baig Mohammad, School of Electronics and Communication Engineering, REVA University, Bangalore, India, E-mail: alibaig.mohammad@reva.edu.in
Shaik Hasane Ahammad, Department of ECE, Koneru Lakshmaiah Education Foundation, Vaddeswaram, Andhra Pradesh 522302, India, E-mail: ahammadklu@gmail.com
Farid Anwar Fawzy, Electronics and Electrical Communications Engineering Department Faculty of Electronic Engineering, Menoufia University, Menouf 32951, Egypt, E-mail: Faridanwar657fawzy@outlook.com

1 Introduction

There are many structures of beams [1–9]. These types includes cantilever, clamped beams, bent beams, folded beams, serpentine beams, and guided beams [10–18]. The cantilever types can be divided into end loading which the cantilever beam (CM) with a point force at the free end can be displayed and analyzed [17, 19–28]. The distributed load which the bending of a CM under its own weight is investigated [29–41]. The mass at free end which the bending of a CM with a mass at the free end and acceleration load which the cantilever with end mass under acceleration is demonstrated [42–53]. The clamped beam (CB) types can be divided into the center loading which the bending of beam forced is observed [54–74].

In this work, the distributed load which the bending of a double CB due to its weight is outlined [75–83]. The central mass can be divided into the distributed load which the bending of a double clamped beam with a central mass is clarified [84–93]. Acceleration load which the double CB with a central mass and the buckling stress which the buckling of a double CB is outlined [94–103]. The bent beam which the design of a corner beam or bent beam suspension is observed. The folded beam which the design of a folded beam suspension for planar motion is outlined [104–114]. The serpentine beam (SM) which the design of a SM suspension is observed [115–128]. The torsion bar which the design of a torsion bar beam suspension is reported. The guided beam which the design of a guided beam hammock suspension and guide beam are reported. The crab leg flexure which the design of a crab leg suspension through the crab leg and the folded flexure through the design of a folded flexure suspension through the flexure are reported in the simulation results [129–153].

2 Models performance parameters and discussions

Figure 1(a) clarifies the bending of a CB with a point force at the free end. Where the cantilever length, width, and thickness are 500 μm, 100 μm, and 5 μm, force at free end is 5 μN, Young's modulus (YM) is 180 GPa. As the length of cantilever increases, this results in the decrease of the deflection of a cantilever.

The obtained results clarified the tip deflection is 1.111 μm, the maximum stress is 6 MPa, and the spring

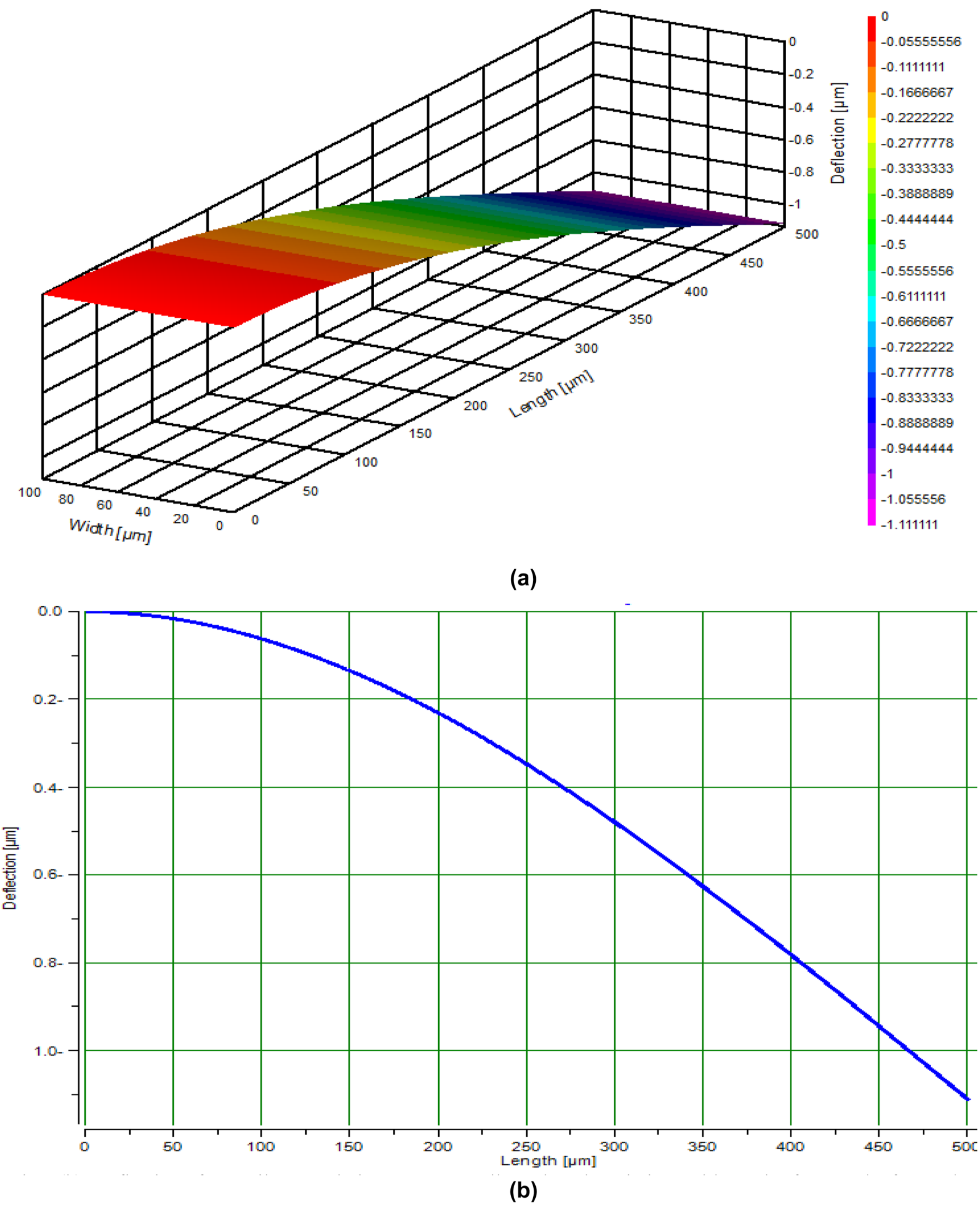

Figure 1: Cantilever deflection variations against length. (a) Cantilever deflection with a point force at the free end. (b) Deflection of cantilever variations versus cantilever length variations with a point force at the free end.

constant is 4.5 N/m. Figure 1(b) outlines the deflection of a cantilever variations versus cantilever length variations with a point force at the free end. It is demonstrated that the deflection of a cantilever decreases with the increase of cantilever length.

Figure 2(a) outlines the bending of a cantilever due to the distributed weight of the beam. Where the length of cantilever is 1000 μm, cantilever width is 500 μm, cantilever thickness is 10 μm, the density is 2330 kg/m^3, and Young's modulus is 180 GPa. The clarified results show that the tip deflection is 1.903 E-003 μm, the maximum stress is 6.850 E-003 MPa, the spring constant is 22.5 N/m. Figure 2(b) shows the deflection of a cantilever variations against cantilever length variations due to the distributed weight at the beam. It is clear that the deflection of a cantilever decreases with the increase of cantilever length.

Figure 3(a) clarifies the bending of a cantilever due to a mass at the free end. Where the cantilever length, width, and thickness are 400 μm, 100 μm, and 5 μm, Mass at free end is 4E-06 kg, and YM is 180 GPa. The clarified results show that the tip deflection is 4.46 μm, the maximum stress is 37.632 MPa, and the spring constant is 8.79 N/m. Figure 1(b)

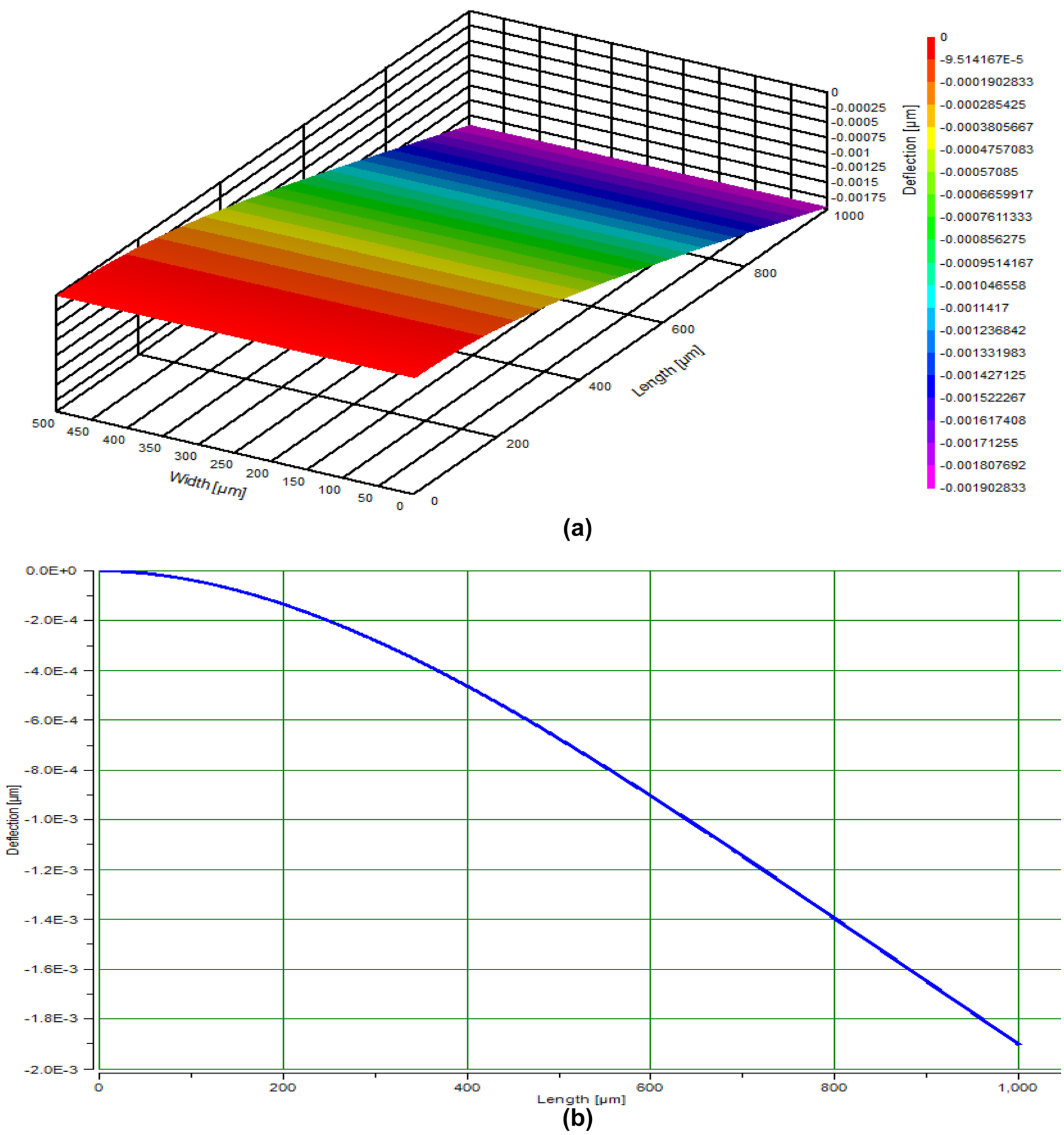

Figure 2: Deflection against cantilever. (a) Deflection of a cantilever due to the distributed weight at the beam. (b) Deflection of cantilever variations versus cantilever length variations.

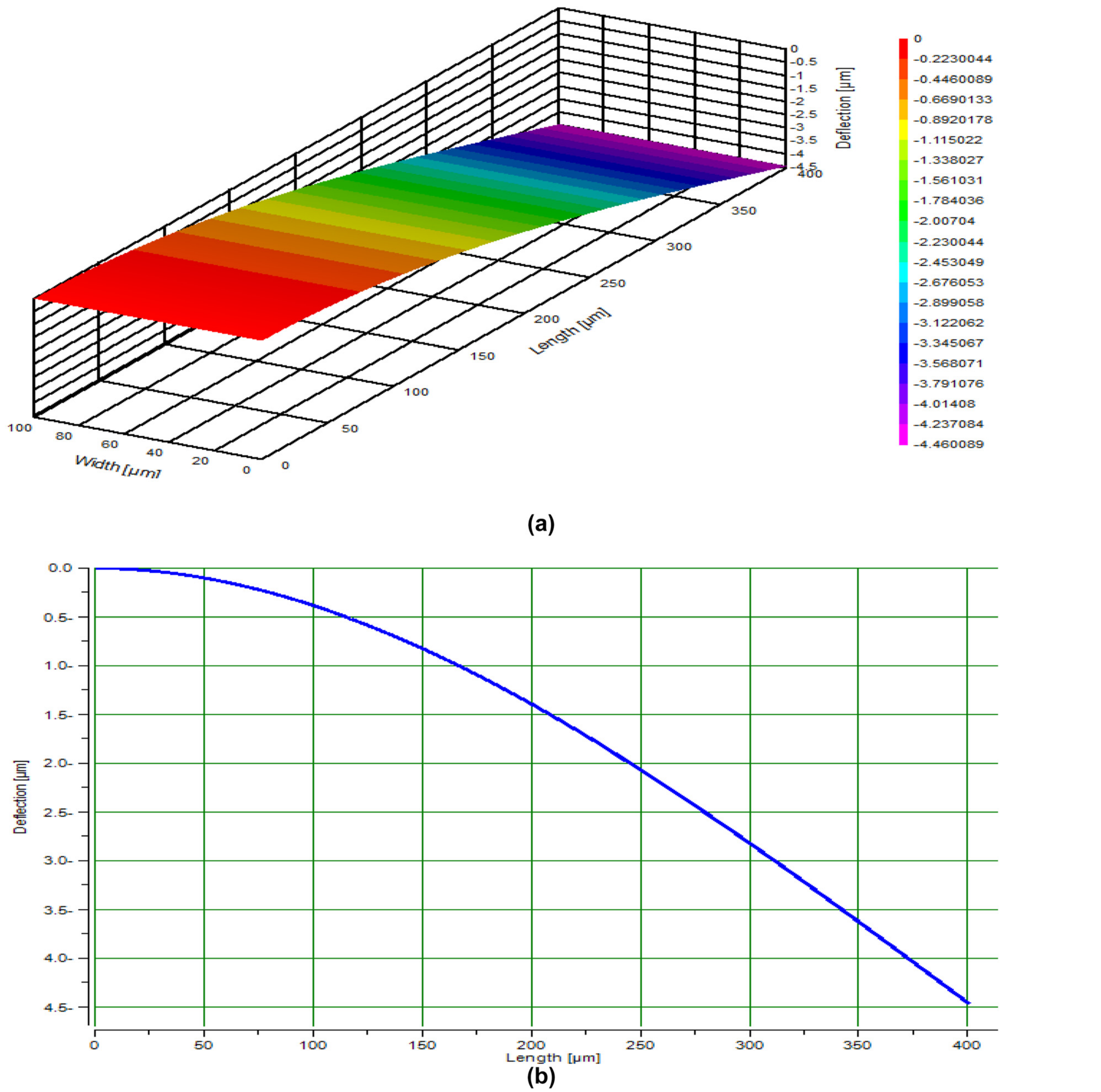

Figure 3: Cantilever deflection variations against Cantilever length. (a) Deflection of a cantilever with a mass at the free end. (b) Deflection of cantilever variations versus cantilever length variations with a mass at the free end.

outlines the deflection of a cantilever variations versus cantilever length variations with a mass at the free end. It is demonstrated that the deflection of a cantilever decreases with the increase of cantilever length.

Figure 4(a) outlines the cantilever with a mass at the free end under acceleration. Where the beam length, width, and thickness are 400 µm, 100 µm, and 5 µm, mass at free end is 4E-06 kg, acceleration is 10 g, and YM is 180 GPa. It is clear that from the results that the maximum deflection is 44.601 µm, the maximum stress is 376.32 MPa, and the maximum strain is 2090.7 microstrains. Figure 4(b) outlines the maximum stress versus acceleration for a cantilever mass structure. The maximum stress increases as the acceleration increases.

Figure 5(a) shows the deflection of a BC at both ends with a force at the center. Where the beam length, width, and thickness are 525 µm, 250 µm, and 5 µm, the force at center is 100 µN, and Young's modulus is 180 GPa. The clarified results assured that the tip deflection is 0.1608 µm, the maximum stress is 6.3 MPa, and the spring constant is

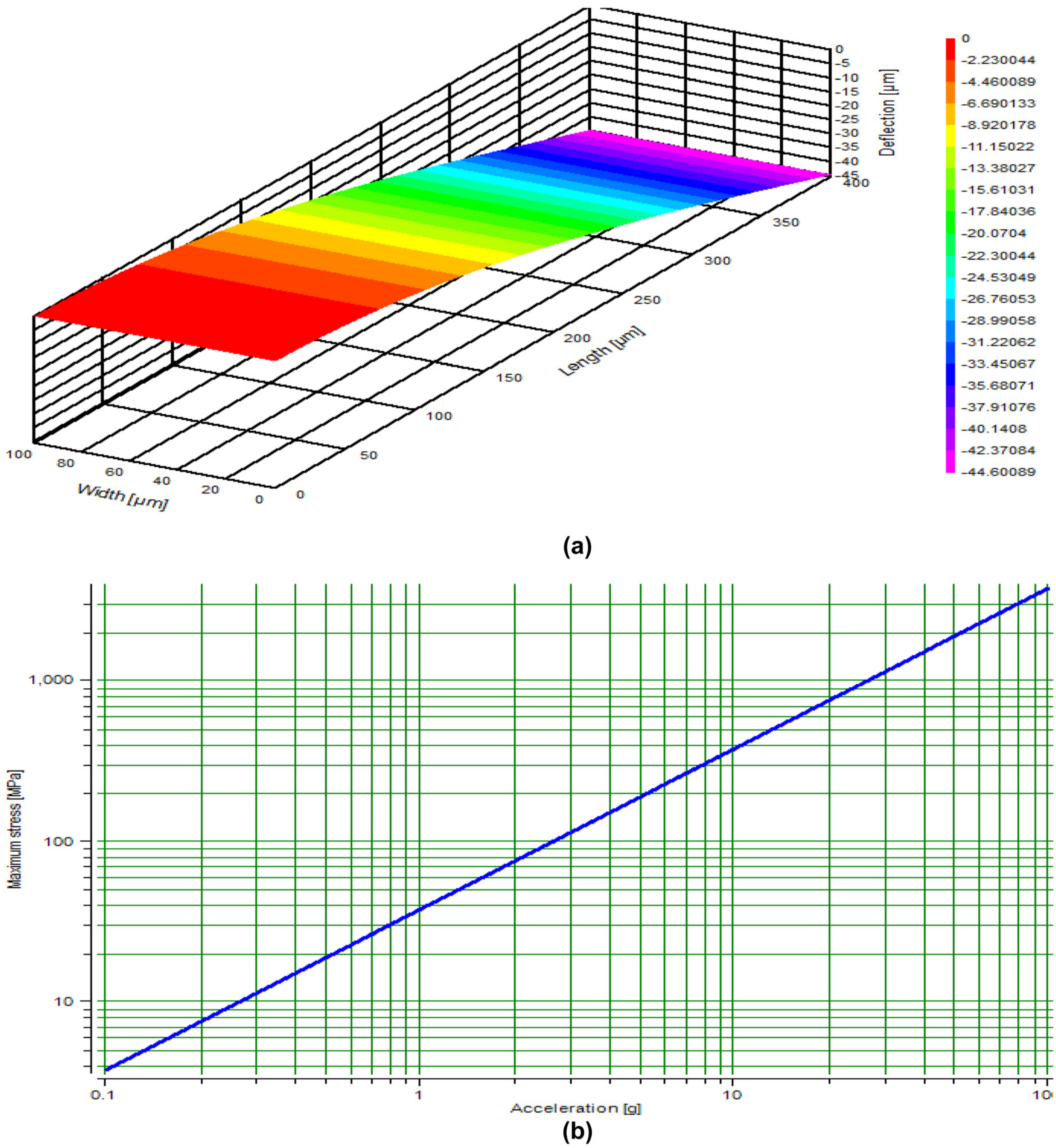

Figure 4: Maximum stress variations against acceleration variations. (a) Deflection of a cantilever at the free end under acceleration. (b) Maximum stress versus acceleration for a cantilever mass structure.

621.963 N/m. Figure 5(b) shows the beam clamped deflection variations with the length beam variations based a force at the center. As the beam length changes from 1 to 275 μm, this results in the decreases of deflection of a beam exponentially. But as the beam length changes from 275 to 525 μm, this results in the increases of deflection of a beam exponentially.

Figure 6(a) outlines the bending of a double CB under its distributed weight. Where the beam length, width, and thickness are 835 μm, 125 μm, and 7.5 μm, the density is 2330 kg/m^3, and YM is 180 GPa. The simulation results assured that the tip deflection is 3.426 E-005 μm, the maximum stress is 1.061 E-003 MPa, and the spring constant is 260.872 N/m. As the length of beam varies from 1 to 425 μm, this results in the decreases of deflection of a beam exponentially. But as the length of beam varies from 425 to 835 μm, this results in the increases of deflection of a beam exponentially.

Figure 7(a) clarifies the deflection of a double CB with a central mass under its weight. Where the beam length, width, and thickness are 400 μm, 100 μm, and 5 μm, the mass length is 1500 μm, the mass width is 1500 μm, the mass

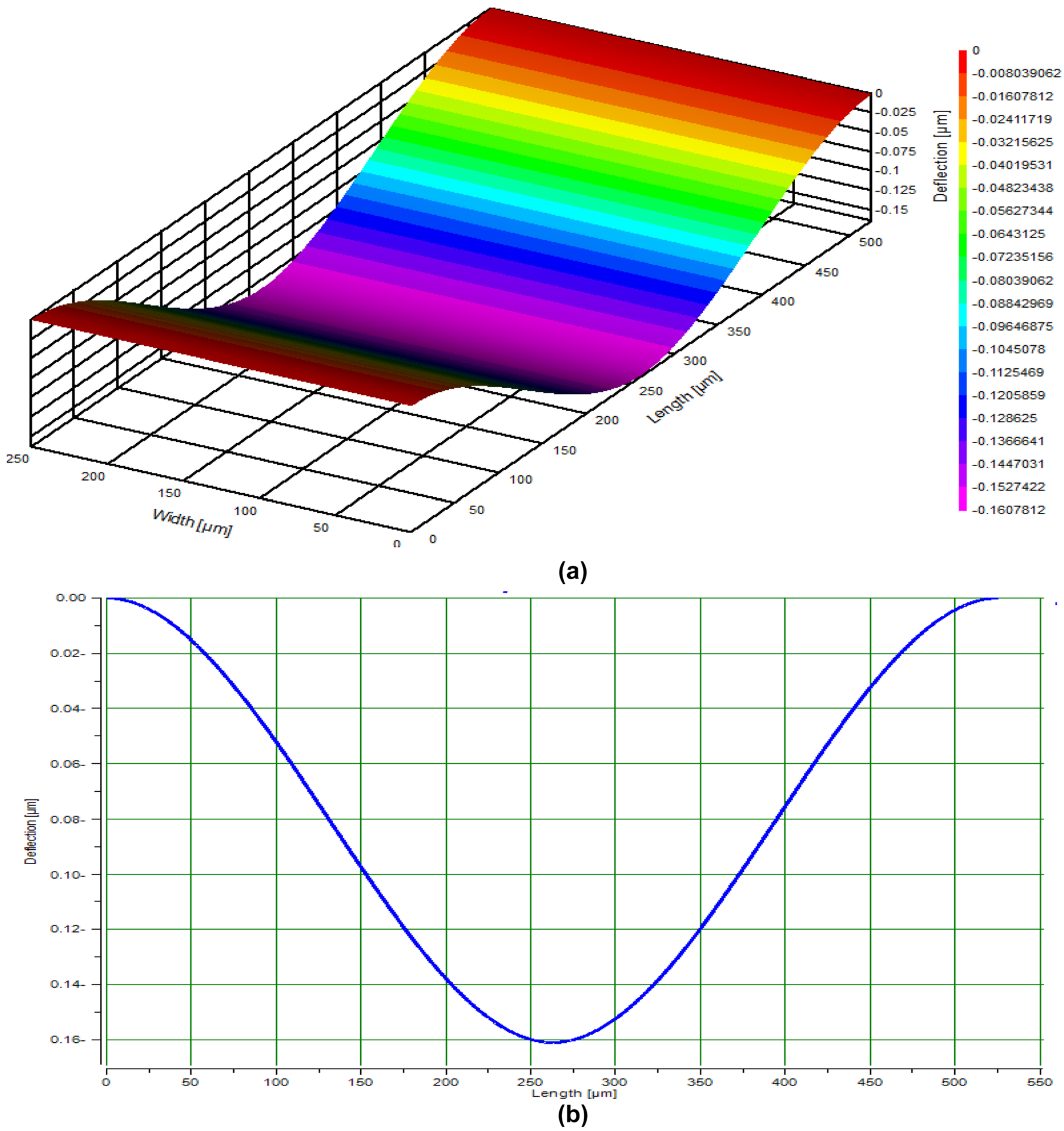

Figure 5: Beam clamped deflection variations versus Cantilever length. (a) Deflection of a beam clamped (BC) at both ends with force at the center. (b) Deflection of BC variations with the beam length variations at both ends with a force at the center.

thickness is 400 µm, density is 2330 kg/m^3, and Young's modulus is 180 GPa. The simulation results indicates that the deflection of the central mass is 0.292 µm, The maximum stress is 4.934 MPa, and The spring constant is 70.312 N/m. Figure 7(b) shows the stress on top of a double CB with a central mass under its weight in the relation to beam length. The stress decreases linearly with the increase of beam length.

Figure 8(a) clarifies the buckling of a double CB due to a compressive stress. Where the beam length, width, and thickness are 400 µm, 125 µm and 3 µm, compressive stress is 45 MPa, Young's modulus is 180 GPa, and the simulation results show that the buckling stress is 33.276 MPa, the buckling force is 1.248E + 004 µN, and the maximum deflection is 1.678 µm. Figure 8(b). Deflection or Buckling of a double CB due to a compressive stress in relation to beam length. The Deflection or Buckling of a double CB due to a compressive stress in relation to beam length is clarified in Figure 8(b). The deflection increases exponentially with the increase of beam length up to 200 µm and then

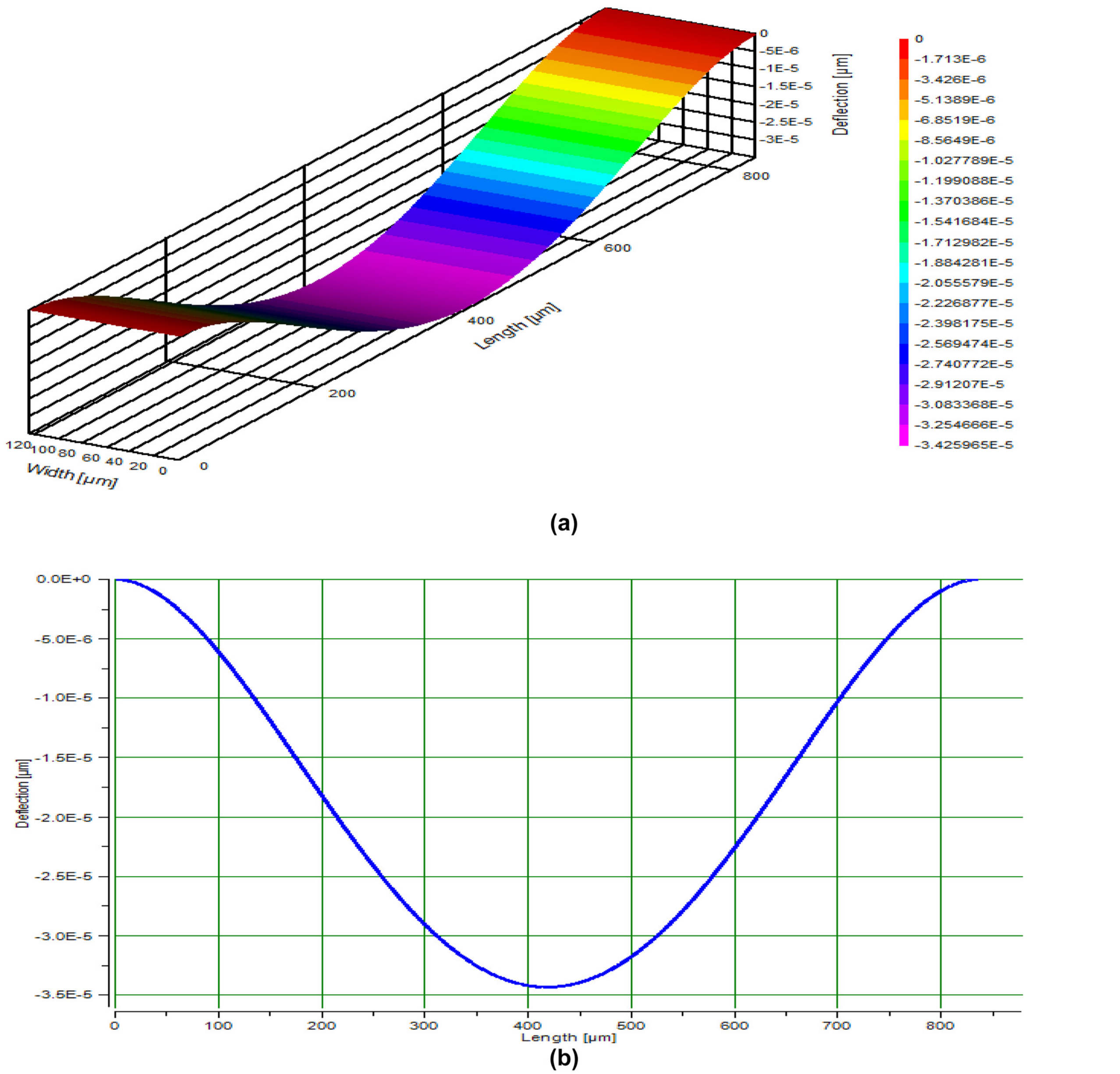

Figure 6: Beam clamped bending variations versus beam length. (a) Bending of a double clamped beam under its distributed weight. (b) Deflection of double CB variations with the beam length variations under its distributed weight.

decreases exponentially with the beam length varies from 200 to 400 µm.

Figure 9(a) outlines the design of a corner beam or bent beam suspension. Where the length of a leg of the beam length, width, and thickness are 40 µm, 5 µm, and 3 µm, YM is 180 GPa, and Poisson's ratio (PR) is 0.3.

The results assured that the spring constant (SC) of a single bent beam in X axis is 650.55 N/m, the SC of a single bent beam in Y axis is 650.55 N/m, and the SC of a single bent beam in Z axis is 35.13 N/m. The effect of beam design on in plane stiffness of a bent beam is clarified in Figure 9(b). The SC in x-direction decreases linearly with (length/width) ratio of beam variations. Figure 10(a) outlines the design of a folded beam suspension for planar motion. Where the first leg beam length is 50 µm, second leg beam length is 30 µm, third leg beam length is 85 µm, beam width is 15 µm, beam thickness is 5 µm, YM is 180 GPa, and PR is 0.3.

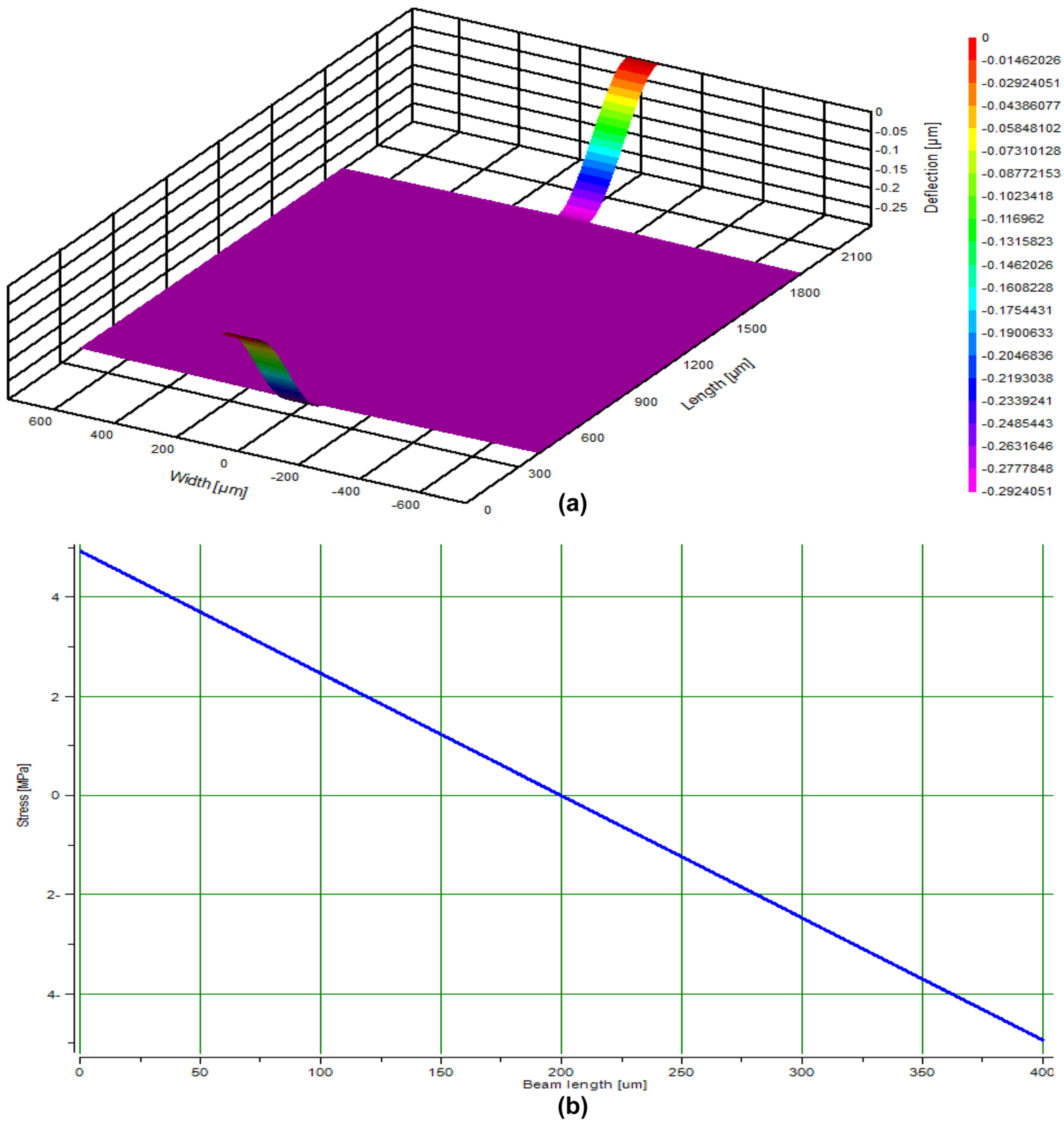

Figure 7: Beam clamped deflection variations versus cantilever length. (a) Deflection of a double CB with a central mass under its weight. (b) Stress on top of a double CB with a central mass under its weight in the relation to beam length.

The simulation results assured that the SC of a single beam in X axis is 1466.329 N/m, The SC of a single beam in Y axis is 2960.526 N/m, and SC of a single beam in Z axis is 206.045 N/m. Figure 10(b) clarifies out of plane deflection of a folded beam suspension. The SC decreases linearly with beam (length 2/length 1) [%] in all x, y, and z directions. Figure 11(a) shows the design of a serpentine beam. Where the long arm length beam is 100 µm, the short arm length beam is 20 µm, width beam is 15 µm, thickness beam is 9 µm, YM is 180 GPa, and PR is 0.3.

The simulation results assured that the spring constant in X for one beam is 262.861 N/m, The SC in Z for one beam is 81.881 N/m, and The torsional spring constant for one beam in X axis is 3.713E + 005 µNµm/rad. Figure 11(b) shows the dependence of stiffness on short leg of the serpentine beam. The spring constant decreases linearly

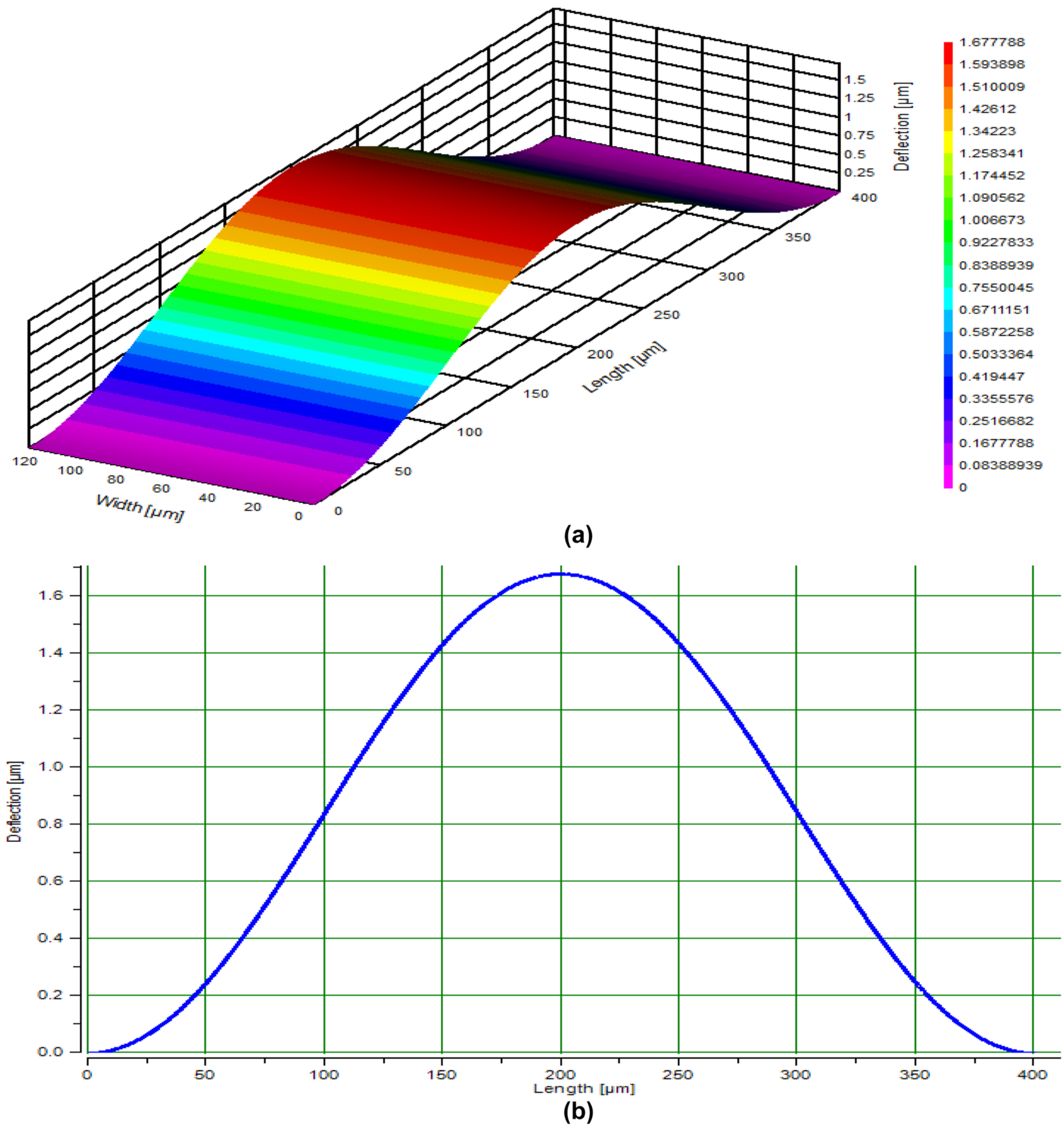

Figure 8: Beam clamped buckling variations versus beam length. (a) Buckling of a double CB due to a compressive stress. (b) Deflection or buckling of a double CB due to a compressive stress in relation to beam length.

with beam (length 2/length 1) [%] in all *x*, *y*, and *z* directions. Figure 12 clarifies the design of a torsion bar beam suspension. Where the beam length is 100 μm, longer shorter side of cross section are 40 and 9 μm, applied torque is 350,000 μNμm, YM is 180 GPa, and PR is 0.3.

The results show that the torsional stiffness constant is 5.773E + 006 μNμm/rad, and the maximum shearing stress is 377.209 MPa. The Figure also clarifies the dependence of cross section of beam on torsion constant and the relation between the spring constant and shorter/longer side length is also clarified. As longer/shorter side length ratio increases, this results in the increase of the spring constant. Figure 13 shows the design of a guided beam hammock suspension. Where the beam length is 750 μm, the beam width is 5 μm, the beam thickness is 15 μm, and YM is 180 GPa. The Stiffness ratio of lateral to vertical motion of hammock suspension is also clarified.

The results demonstrated that the SC in *X* axis is 3.2 N/m, the spring constant in *Y* axis is 18,000 N/m, and The SC in *Z* axis is 28.8 N/m. The lateral shiftiness/out of plane shiftiness

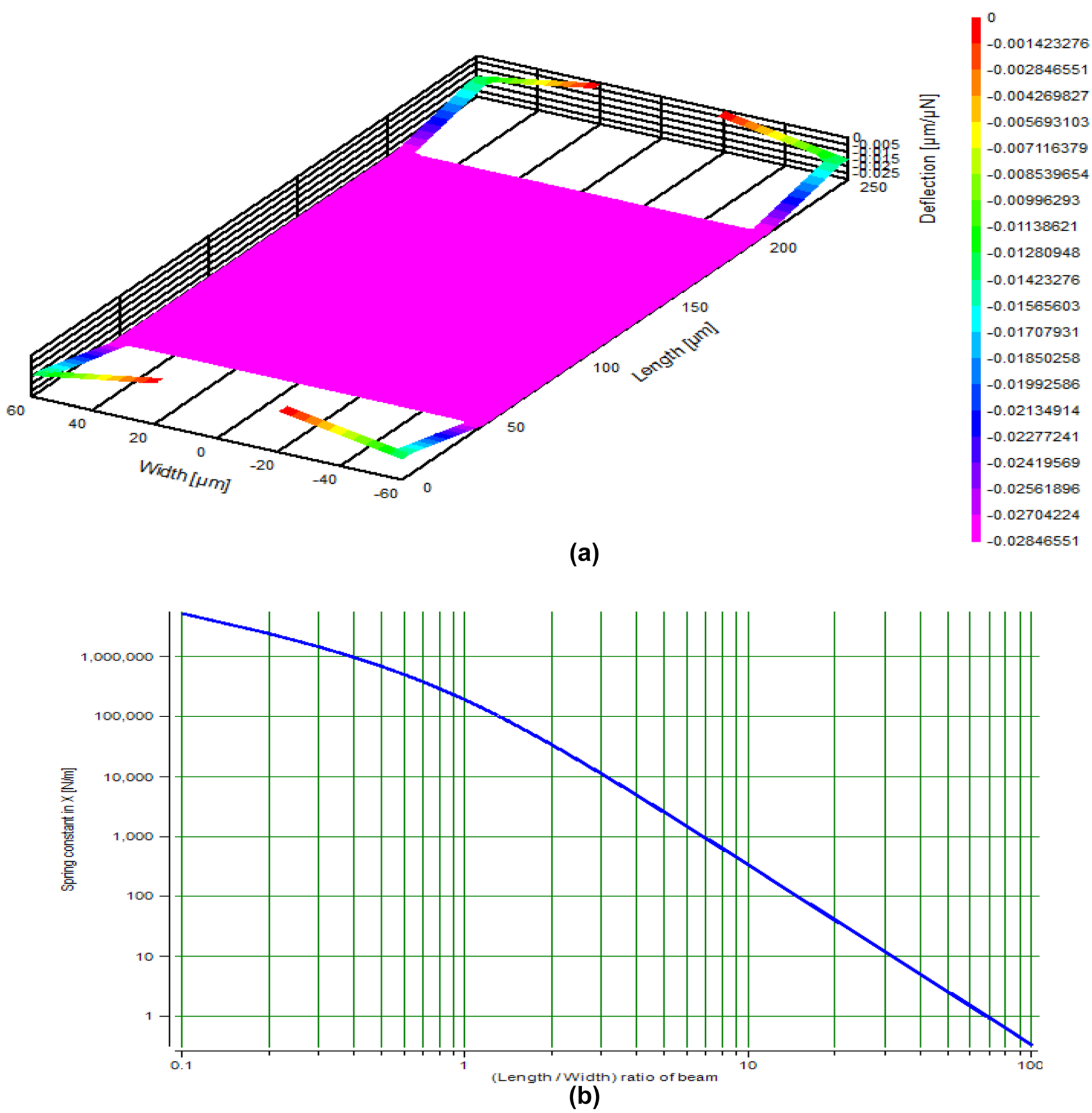

Figure 9: Beam bent suspension variations versus beam dimensions. (a) Out of plane deflection of a bent beam suspension. (b) Spring constant in *x*-direction variations in relation to length/width ratio of beam.

ratio increases as the beam width to thickness ratio also increases. Figure 14 shows the design of a crab-leg suspension and the dependence of the stiffness on thigh section of the crab leg flexure. Where the shin leg beam length is 150 µm, the shin leg beam width is 10 µm, the thigh leg beam length is 100 µm, width of thigh leg of beam is 10 µm, thickness of beam is 5 µm, YM is 180 GPa, and PR is 0.3.

The results assured that the SC of the suspension in X axis is 746.667 N/m, the SC of the suspension in Y axis is 1980 N/m, and the SC of the suspension in Z axis is 89.471 N/m. The SC decreases linearly in x and y directions as thigh length increases. Also the spring constant decreases exponentially in z direction as thigh length increases. Figure 15 outlines the design of a folded flexure suspension and the dependence of stiffness on ratio of column beam lengths. Where the length of outer column beam is 100 µm, length of inner column beam is 100 µm, width of column beam is 5 µm, length of outer truss beam is 95 µm, length of inner truss beam is 95 µm, width of truss beam is 5 µm, beam thickness is 12 µm, YM is 160 GPa, and PR is 0.3.

The results clarified that the spring constant of the suspension in X axis is 306.736 N/m, the SC of the suspension in Y axis is 489.056 N/m, and the SC of the suspension in Z axis is 425.668 N/m. The spring constant decreases linearly for all x, y, z directions with the column beam length ratio [inner/outer].

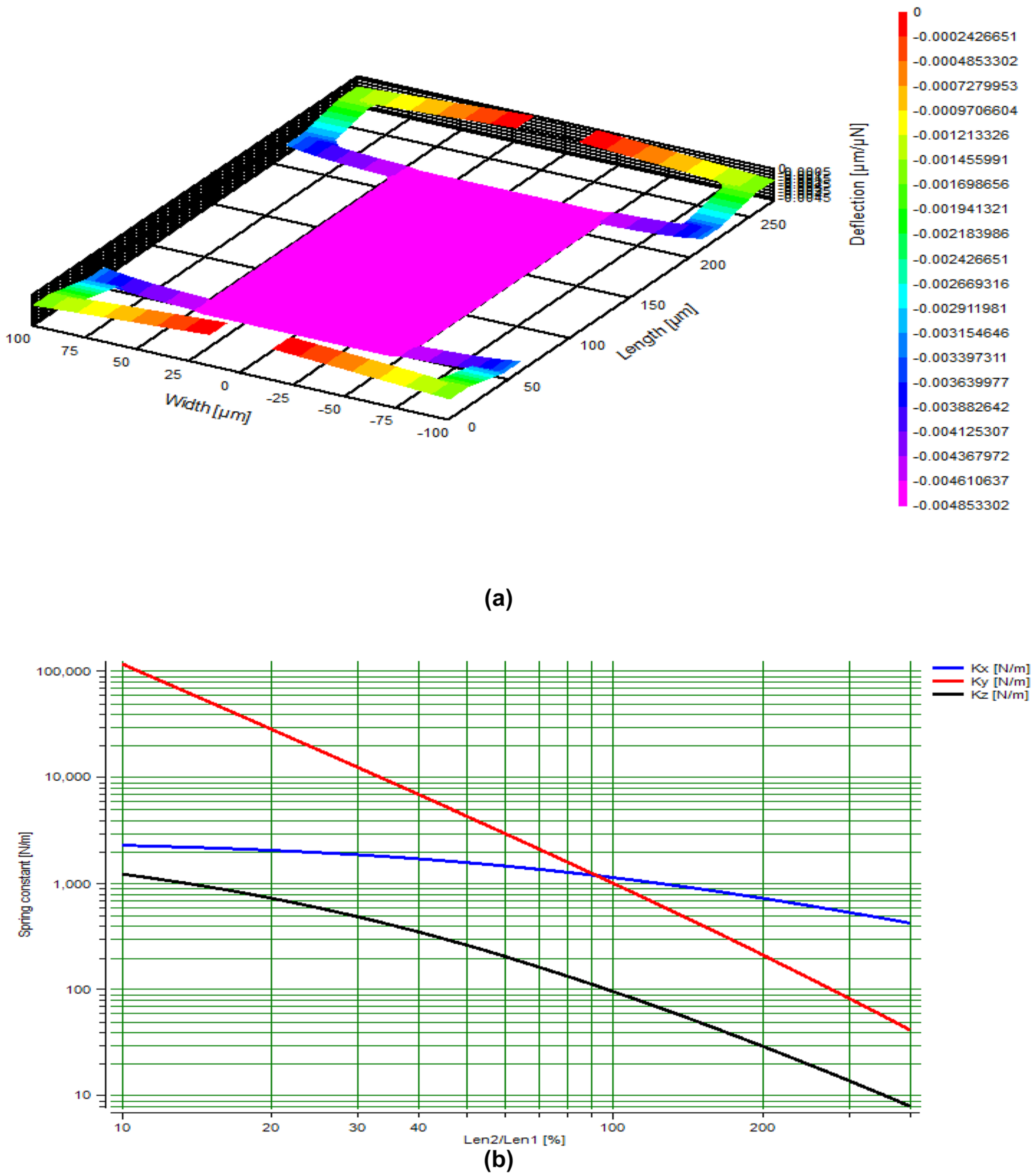

Figure 10: Plane deflection variations versus folded beam dimensions. (a) Out of plane deflection of a folded beam suspension. (b) Dependence of stiffness on mid-section of the folded beam.

3 Conclusions

We have outlined the review study on different guided beams surface structure mechanics in MEMS by using MEMSolver simulation. The design of a crab-leg suspension and the dependence of the stiffness on thigh section of the crab leg flexure is clarified. The design of a folded flexure suspension and the dependence of stiffness on ratio of column beam lengths is demonstrated. Besides the design of a guided beam hammock suspension, the design of a serpentine beam and the design of a torsion bar beam suspension are presented. The design of a folded beam suspension for planar motion, the design of a corner beam or bent beam suspension, the buckling of a double CB due to a compressive

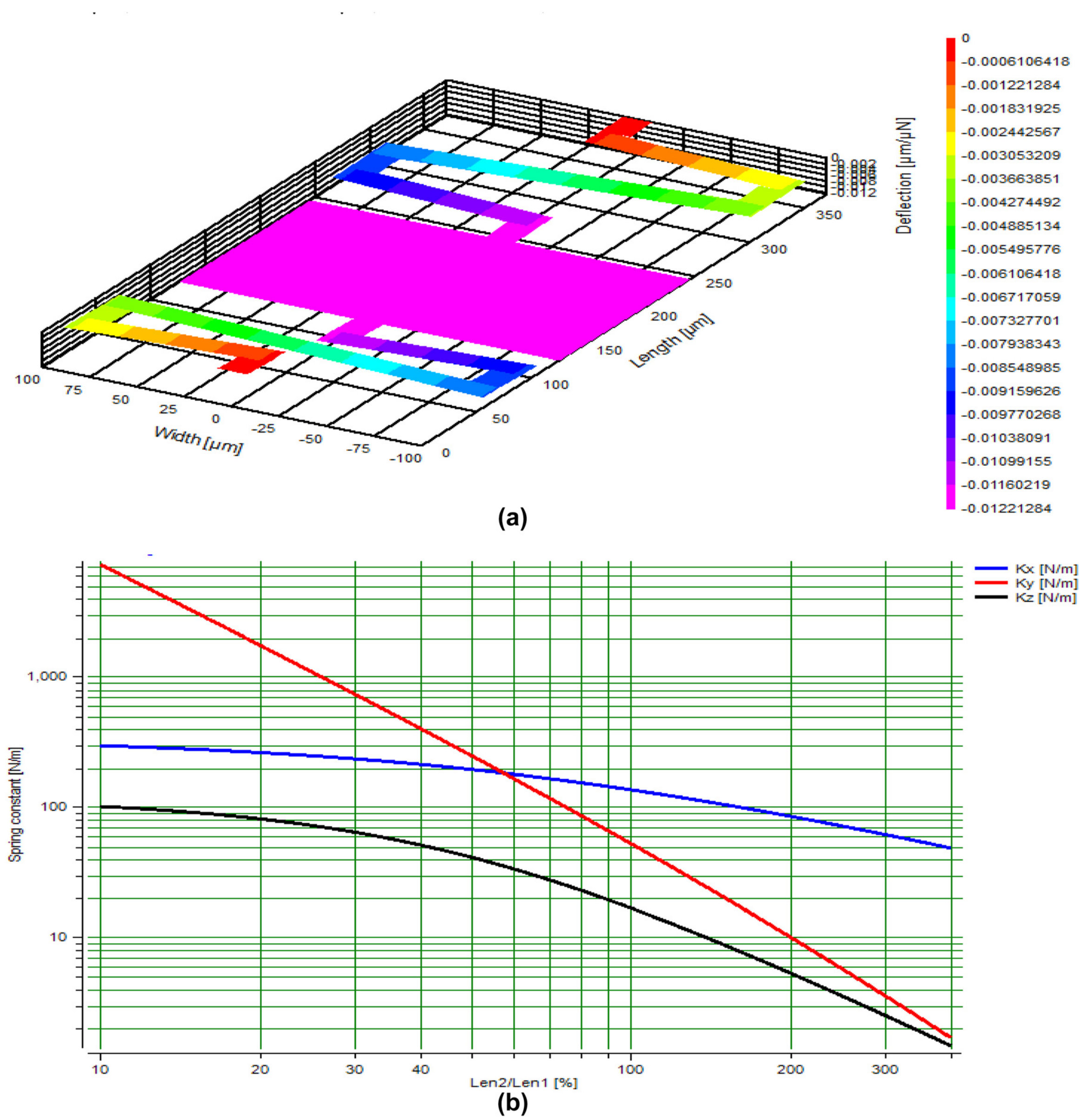

Figure 11: Plane deflection variations versus short leg of serpentine length. (a) Out of plane deflection of a serpentine beam suspension. (b) Dependence of stiffness on short leg of the serpentine beam.

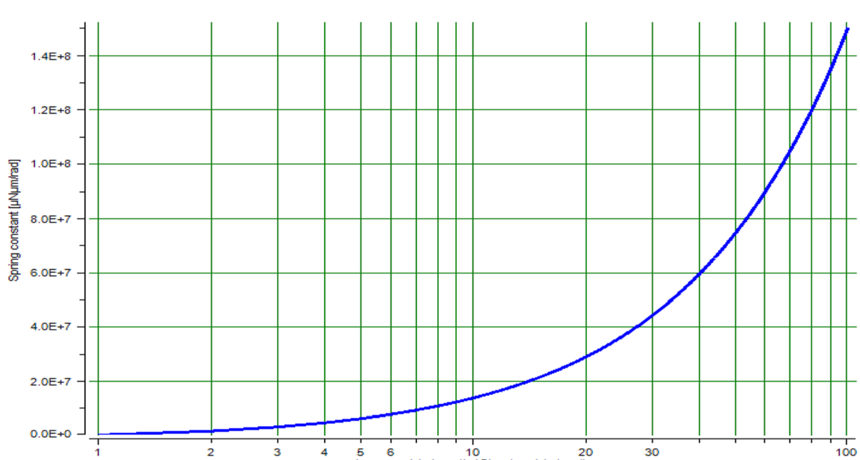

Figure 12: Dependence of cross section of beam on torsion constant.

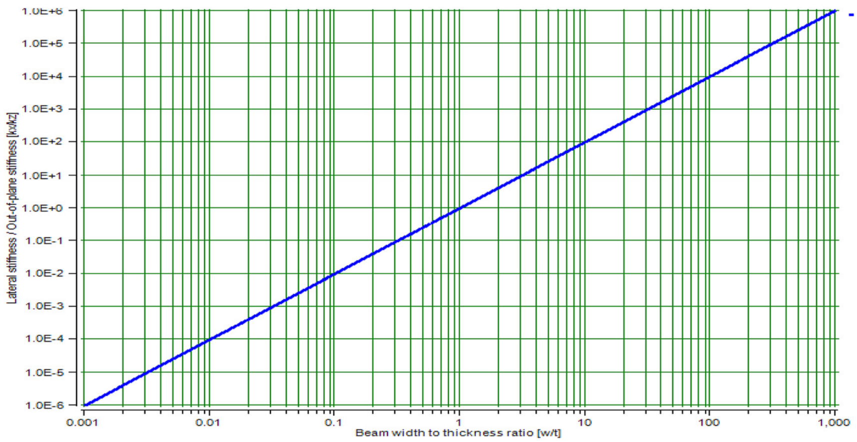

Figure 13: Stiffness ratio of lateral to vertical motion of hammock suspension.

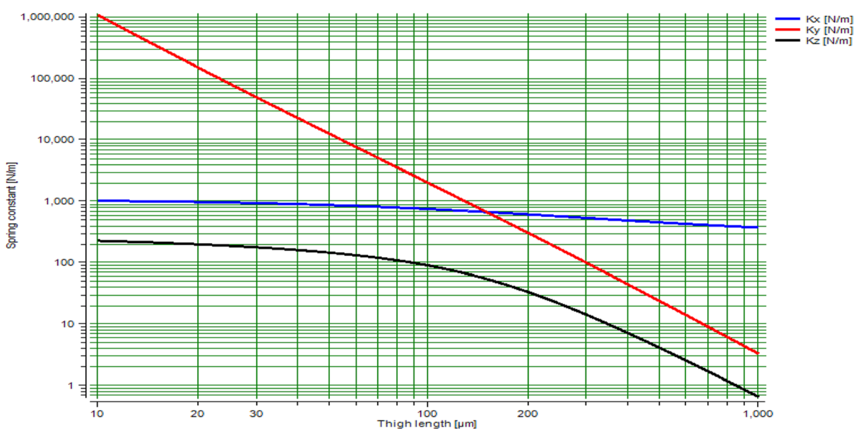

Figure 14: Spring constant variations in various *x*, *y*, and *z* directions against thigh length.

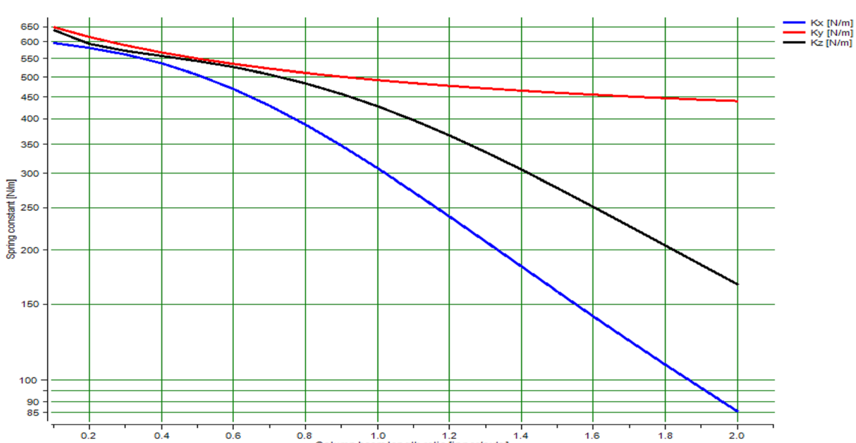

Figure 15: Spring constant versus column beam length ratio [inner/outer] in various *x*, *y*, and *z* directions.

stress, the deflection of a double CB with a central mass under its weight, and the bending of a double clamped beam under its distributed weight are demonstrated.

Author contributions: All the authors have accepted responsibility for the entire content of this submitted manuscript and approved submission.
Research funding: None declared.
Conflict of interest statement: The authors declare no conflicts of interest regarding this article.

References

1. Tahhan SR, Taha RM. Mercedes Benz logo based plasmon resonance PCF sensor. Sens Bio-Sens Res 2021;35:1–9.

2. Tahhan SR, Mohammed MF, Moosa AA, Atieh A. WDM ROF OFDM/QAM system for wireless PON. In: Jordan international joint conference on electrical engineering and information technology (JEEIT); 2021, vol 10:1–14 pp.
3. Tahhan SR, Ahmad A, Hasan M, Hall T. Characterization and experimental verification of actively mode-locked erbium doped fiber laser utilizing ring cavity. Tech Mess 2020;9:1–7.
4. Fadil EA, Abass AK, Tahhan SR. Secure WDM-free space optical communication system based optical chaotic. Opt Quant Electron 2022;54:1–14.
5. Amin R, Abdulrazak LF, Tahhan SR, Mohammadd N, Ahmed K, Bui4 FM, et al. Tellurite glass based optical fiber for the investigation of supercontinuum generation and nonlinear properties. Phys Scripta 2022;97:1402–4896.
6. Tahhan SR, Atieh A, Ali MH, Hasan M, Abass AK, Hall T. Characteristics of actively mode-locked erbium doped fiber laser utilizing ring cavity. In: Jordan international joint conference on electrical engineering and information technology (JEEIT); 2019, vol 10:1–15 pp.
7. Tahhan SR, Hasen F. Longitudinal characterization of fiber Bragg gratings. J Opt 2022;45:1–12.
8. Mohammadda N, Abdulrazak LF, Tahhanc SR, Amina R, Ibrahimd SM, Ahmede K, et al. GaP-filled PCF with ultra-high birefringence and nonlinearity for distinctive optical applications. J Ovonic Res 2022;18:129–40.
9. Ahammad SH, Rajesh V, Rahman MZU, Lay-Ekuakille A. A hybrid CNN-based segmentation and boosting classifier for real time sensor spinal cord injury data. IEEE Sensor J 2020;20:10092–101.
10. Ahammad SH, Rajesh V, Rahman MZU. Fast and accurate feature extraction-based segmentation framework for spinal cord injury severity classification. IEEE Access 2019;7:46092–46.
11. Ahammad SH, Rahman MZU, Koteswara Rao L, Sulthana A, Gupta N, Lay-Ekuakille A. A multi-level sensor-based spinal cord disorder classification model for patient wellness and remote monitoring. IEEE Sensor J 2020;21:14253–62.
12. Ahammad SH, Rahman MZU, Lay-Ekuakille A, Giannoccaro NI. An Efficient optimal threshold-based segmentation and classification model for multi-level spinal cord Injury detection. In: 2020 IEEE International Symposium on Medical Measurements and Applications (MeMeA). IEEE; 2020:1–6 pp.
13. Inthiyaz S, Prasad MVD, Lakshmi RUS, Sai NTBS, Kumar PP, Ahammad. Agriculture based plant leaf health assessment tool: a deep learning perspective. Int J Emerg Trends Eng Res 2019;7:690–4.
14. Kumar MS, Inthiyaz S, Vamsi CK, Ahammad SH, Lakshmi KS, Gopal PV, et al. Power optimization using dual sram circuit. Int J Innovative Technol Explor Eng 2019;8:1032–6.
15. Ahammad SH, Rajesh V, Hanumatsai N, Venumadhav A, Sasank NSS, Gupta KKB, et al. MRI image training and finding acute spine injury with the help of hemorrhagic and non hemorrhagic rope wounds method. Indian J Public Health Res Dev 2019;10:404–8.
16. Kumar MS, Inthiyaz S, Krishna PV, Ravali CJ, Veenamadhuri J, Reddy YH, et al. Implementation of most appropriate leakage power techniques in vlsi circuits using nand and nor gate. Int J Innovative Technol Explor Eng 2019;8:797–801.
17. Myla S, Marella ST, Goud AS, Ahammad SH, Kumar GNS, Inthiyaz S. Design decision taking system for student career selection for accurate academic system. Int J Sci Technol Res 2019;8:2199–206.
18. Kumar AR, Kumar GNS, Chithanoori JK, Mallik KSK, Srinivas P, Ahammad SH. Design and analysis of a heavy vehicle chassis by using E-glass epoxy & S-2 glass materials. Int J Recent Technol Eng 2019;7:903–5.
19. Gattim NK, Pallerla SR, Bojja P, Reddy TPK, Chowdary VN, Dhiraj V, et al. Plant leaf disease detection using SVM technique. Int J Emerg Trends Eng Res 2019;7:634–7.
20. Reddy KS, Suneela B, Inthiyaz S, Ahammad SH, Kumar GNS, Reddy AM. Texture filtration module under stabilization via random forest optimization methodology. Int J Adv Trends Comput Sci Eng 2019;8:458–69.
21. Narayana VV, Ahammad SH, Chandu BV, Rupesh G, Naidu GA, Gopal GP. Estimation of quality and intelligibility of a speech signal with varying forms of additive noise. Int J Emerg Trends Eng Res 2019;7:430–3.
22. Reddy APC, Kumar MS, Krishna BM, Inthiyaz S, Ahammad SH. Physical unclonable function based design for customized digital logic circuit. Int J Adv Sci Technol 2019;28:206–21.
23. Manohar KRC, Upendar S, Durgesh V, Sandeep B, Mallik KSK, Kumar GNS, et al. Modeling and analysis of kaplan turbine blade using CFD. Int J Eng Technol 2019;7:1086–9.
24. Nagageetha M, Mamilla SK, Ahammad SH. Performance analysis of feedback based error control coding algorithm for video transmission on wireless multimedia networks. J Adv Res Dyn Control Syst 2017;9:626–60.
25. Myla S, Marella ST, Goud AS, Ahammad SH, Kumar GNS, Inthiyaz S. Design decision taking system for student career selection for accurate academic system. Int J Recent Technol Eng 2019;8:2199–206.
26. Reddy KS, Suneela B, Inthiyaz S, Ahammad SH, Kumar GNS, Reddy AM. Texture filtration module under stabilization via random forest optimization methodology. Int J Adv Trends Comput Sci Eng 2021;8:458–69.
27. Murthy ASD, Murthy PS, Rajesh V, Ahammad SH, Jagan BOL. Execution of natural random forest machine learning techniques on multi spectral image compression. Int J Pharm Res 2019;11:1241–55.
28. Kumar AR, Kumar GNS, Chithanoori JK, Mallik KSK, Srinivas P, Ahammad SH. Design and analysis of a heavy vehicle chassis by using E-glass epoxy & S-2 glass materials. Int J Recent Technol Eng 2019;7:903–5.
29. Rashed ANZ, Tabbour MSF, Natarajan K. Performance enhancement of overall LEO/MEO intersatellite optical wireless communication systems. Int J Satell Commun Netw 2020;38:31–40.
30. Amiri IS, Rashed ANZ, Mohammed AEA, El-Din ES, Yupapin P. Spatial continuous wave laser and spatiotemporal VCSEL for high-speed long haul optical wireless communication channels. J Opt Commun 2019;40:320–30.
31. Amiri IS, Rashed ANZ, Yupapin P. Average power model of optical Raman amplifiers based on frequency spacing and amplifier section stage optimization. J Opt Commun 2019;40:340–55.
32. Amiri IS, Houssien FMAM, Rashed ANZ, Mohammed AENA. Temperature effects on characteristics and performance of near-infrared wide bandwidth for different avalanche photodiodes structures. Results Phys 2019;14:102–10.
33. Amiri IS, Rashed ANZ. Simulative study of simple ring resonator-based brewster plate for power system operation stability. Indones J Electr Eng Comput Sci 2019;16:1070–6.
34. Amiri IS, Rashed ANZ. Different photonic crystal fibers configurations with the key solutions for the optimization of data rates transmission. J Opt Commun 2019;40:377–88.
35. Amiri IS, Rashed ANZ, Ramya KC, Kumar KV, Maheswar R. The physical parameters of EDFA and SOA optical amplifiers and bit sequence variations based optical pulse generators impact on the performance of soliton transmission systems. J Opt Commun 2019;40:400–13.

36. Amiri IS, Houssien FMAM, Rashed ANZ, Mohammed AENA. Optical networks performance optimization based on hybrid configurations of optical fiber amplifiers and optical receivers. J Opt Commun 2019; 40:425–36.
37. Amiri IS, Rashed ANZ, Sarker K, Paul BK, Ahmed K. Chirped large mode area photonic crystal modal fibers and its resonance modes based on finite element technique. J Opt Commun 2019;40: 455–65.
38. Amiri IS, Houssien FMAM, Rashed ANZ, Mohammed AENA. Comparative simulation of thermal noise effects for photodetectors on performance of long-haul DWDM optical networks. J Opt Commun 2019;40:477–88.
39. Amiri IS, Rashed ANZ, Mohammed AEA, Aboelazm MB. Single wide band traveling wave semiconductor optical amplifiers for all optical bidirectional wavelength conversion. J Opt Commun 2019;40:503–13.
40. Amiri IS, Rashed ANZ, Mohammed AENA, Zaky WF. Influence of loading, regeneration and recalling elements processes on the system behavior of all optical data bus line system random access memory. J Opt Commun 2019;40:535–44.
41. Malathy S, Kumar KV, Rashed ANZ, Vigneswaran D, Eeldien ES. Upgrading superior operation performance efficiency of submarine transceiver optical communication systems toward multi tera bit per second. Comput Commun J 2019;146:192–200.
42. Amiri IS, Rashed ANZ. Numerical investigation of V shaped three elements resonator for optical closed loop system. Indones J Electr Eng Comput Sci 2019;16:1392–7.
43. Rashed ANZ, Tabbour MSF. The engagement of hybrid dispersion compensation schemes performance signature for ultra wide bandwidth and ultra long haul optical transmission systems. Wirel Pers Commun J 2019;109:2399–410.
44. Rashed ANZ, Tabbour MSF, El-Meadawy S, Anwar T, Sarlan A, Yupapin P, et al. The effect of using different materials on erbium-doped fiber amplifiers for indoor applications. Results Phys 2019;15: 103–10.
45. Amiri IS, Rashed ANZ. Power enhancement of the U-shape cavity microring resonator through gap and material characterizations. J Opt Commun 2019;40:565–78.
46. Amiri IS, Kuppusamy PG, Rashed ANZ, Jayarajan P, Thiyagupriyadharsan MR, Yupapin P. The engagement of hybrid ultra high space division multiplexing with maximum time division multiplexing techniques for high-speed single-mode fiber cable systems. J Opt Commun 2019;40:588–603.
47. Amiri IS, Rashed ANZ, Jahan S, Paul BK, Ahmed K. Polar polarization mode and average radical flux intensity measurements based on all optical spatial communication systems. J Opt Commun 2019;40: 618–28.
48. Sivaranjani S, Sampathkumar A, Rashed ANZ, Sundararajan TVP, Amiri IS. Performance evaluation of bidirectional wavelength division multiple access broadband optical passive elastic networks operation efficiency. J Opt Commun 2019;40:645–60.
49. Amiri IS, Rashed ANZ, Yupapin P. High-Speed transmission circuits signaling in optical communication systems. J Opt Commun 2019;40: 675–88.
50. Amiri IS, Rashed ANZ, Jahan S, Paul BK, Ahmed K, Yupapin P. Technical specifications of the submarine fiber optic channel bandwidth/ capacity in optical fiber transmission systems. J Opt Commun 2019;40: 701–15.
51. Amiri IS, Rashed ANZ. Signal processing criteria based on electro-optic filters for fiber optic access transceiver systems. J Opt Commun 2019; 40:733–42.
52. Amiri IS, Rashed ANZ, Yupapin P. Pump laser automatic signal control for erbium-doped fiber amplifier gain, noise figure, and output spectral power. J Opt Commun 2019;40:755–70.
53. Amiri IS, Rashed ANZ, Parvez AHMS, Paul BK, Ahmed K. Performance enhancement of fiber optic and optical wireless communication channels by using forward error correction codes. J Opt Commun 2019;40:786–803.
54. Amiri IS, Rashed ANZ, Yupapin P. Z Shaped like resonator with crystal in the presence of flat mirror based standing wave ratio for optical antenna systems. Indones J Electr Eng Comput Sci 2020;17:1405–9.
55. Amiri IS, Rashed ANZ, Yupapin P. Influence of device to device interconnection elements on the system behavior and stability. Indones J Electr Eng Comput Sci 2020;18:843–7.
56. Eid MMA, Amiri IS, Rashed ANZ, Yupapin P. Dental lasers applications in visible wavelength operational band. Indones J Electr Eng Comput Sci 2020;18:890–5.
57. Amiri IS, Rashed ANZ, Yupapin P. Comparative simulation study of multi stage hybrid all optical fiber amplifiers in optical communications. J Opt Commun 2020;41:12–28.
58. Amiri IS, Rashed ANZ, Kader HMA, Al-Awamry AA, El-Aziz IAA, Yupapin P, et al. Optical communication transmission systems improvement based on chromatic and polarization mode dispersion compensation simulation management. Optik J 2019;207:163–72.
59. Samanta D, Sivaram M, Rashed ANZ, Boopathi CS, Amiri IS, Yupapin P. Distributed feedback laser (DFB) for signal power amplitude level improvement in long spectral band. J Opt Commun 2020;41:33–43.
60. Amiri IS, Rashed ANZ, Yupapin P. Analytical model analysis of reflection/transmission characteristics of long-period fiber bragg grating (LPFBG) by using coupled mode theory. J Opt Commun 2020; 41:55–70.
61. Amiri IS, Rashed ANZ, Rahman Z, Paul BK, Ahmed K. Conventional/ phase shift dual drive Mach–Zehnder modulation measured type based radio over fiber systems. J Opt Commun 2020;41:85–100.
62. Alatwi AM, Rashed ANZ, El-Eraki AM, Amiri IS. Best candidate routing algorithms integrated with minimum processing time and low blocking probability for modern parallel computing systems. Indones J Electr Eng Comput Sci 2020;19:847–54.
63. El-Hageen HM, Alatwi AM, Rashed ANZ. Silicon-Germanium dioxide and aluminum indium gallium arsenide-based acoustic optic modulators. Open Eng J 2020;10:506–11.
64. El-Hageen HM, Alatwi AM, Rashed ANZ. RZ line coding scheme with direct laser modulation for upgrading optical transmission systems. Open Eng J 2020;10:546–51.
65. Alatwi AM, Rashed ANZ, El-Gammal EM. Wavelength division multiplexing techniques based on multi transceiver in low earth orbit intersatellite systems. J Opt Commun 2020;41:113–22.
66. El-Hageen HM, Kuppusamy PG, Alatwi AM, Sivaram M, Yasar ZA, Rashed ANZ. Different modulation schemes for direct and external modulators based on various laser sources. J Opt Commun 2020;41: 132–40.
67. El-Hageen HM, Alatwi AM, Rashed ANZ. High-speed signal processing and wide band optical semiconductor amplifier in the optical communication systems. J Opt Commun 2020;41:155–70.
68. El-Hageen HM, Alatwi AM, Rashed ANZ. Laser measured rate equations with various transmission coders for optimum of data transmission error rates. Indones J Electr Eng Comput Sci 2020;20: 1406–12.
69. Eid MMA, Habib MA, Anower MS, Rashed ANZ. Highly sensitive nonlinear photonic crystal fiber based sensor for chemical sensing applications. Microsyst Technol J 2021;27:1007–14.

70. Eid MMA, Rashed ANZ, Shafkat A, Ahmed K. Fabry Perot laser properties with high pump lasers for upgrading fiber optic transceiver systems. J Opt Commun 2020;41:188–200.
71. Eid MMA, Rashed ANZ, Hosen MS, Paul BK, Ahmed K. Spatial optical transceiver system–based key solution for high data rates in measured index multimode optical fibers for indoor applications. J Opt Commun 2020;41:213–22.
72. Eid MMA, Rashed ANZ, El-Meadawy S, Ahmed K. Simulation study of signal gain optimization based on hybrid composition techniques for high speed optically dense multiplexed systems. J Opt Commun 2020; 41:235–50.
73. Alatwi AM, Rashed ANZ. Hybrid CPFSK/OQPSK modulation transmission techniques' performance efficiency with RZ line coding–based fiber systems in passive optical networks. Indones J Electr Eng Comput Sci 2021;21:263–70.
74. Alatwi AM, Rashed ANZ. An analytical method with numerical results to be used in the design of optical slab waveguides for optical communication system applications. Indones J Electr Eng Comput Sci 2021;21:278–86.
75. Alatwi AM, Rashed ANZ. Conventional doped silica/fluoride glass fibers for low loss and minimum dispersion effects. Indones J Electr Eng Comput Sci 2021;21:287–95.
76. El-Hageen HM, Alatwi AM, Rashed ANZ. Spatial optical transmitter based on on/off keying line coding modulation scheme for optimum performance of telecommunication systems. Indones J Electr Eng Comput Sci 2021;21:305–12.
77. Eid MMA, Rashed AANZ, Kurmendra. High speed optical switching gain based EDFA model with 30 Gb/s NRZ modulation code in optical systems. J Opt Commun 2020;41:288–300.
78. Eid MMA, Rashed ANZ, Amiri IS. Fast speed switching response and high modulation signal processing bandwidth through LiNbO3 electro-optic modulators. J Opt Commun 2020;41:312–25.
79. Eid MMA, Houssien FMAM, Rashed ANZ, Mohammed AENA. Performance enhancement of transceiver system based inter satellite optical wireless channel (IS-OWC) for ultra long distances. J Opt Commun 2020;41:345–60.
80. Eid MMA, Rashed ANZ, El-Din ES. Simulation performance signature evolution of optical inter satellite links based booster EDFA and receiver preamplifiers. J Opt Commun 2020;41:388–400.
81. Eid MMA, Rashed ANZ, El-Gammal EM. Influence of dense wavelength division multiplexing (DWDM) technique on the low earth orbit intersatellite systems performance. J Opt Commun 2020;41:412–26.
82. Eid MMA, Rashed ANZ, Bulbul AAM, Podder E. Mono rectangular core photonic crystal fiber (MRC-PCF) for skin and blood cancer detection. Plasmonics J 2021;16:717–27.
83. Eid MMA, Seliem AS, Rashed ANZ, Mohammed AENA, Ali MY, Abaza SS. High speed pulse generators with electro-optic modulators based on different bit sequence for the digital fiber optic communication links. Indones J Electr Eng Comput Sci 2021;21:957–67.
84. Eid MMA, Seliem AS, Rashed ANZ, Mohammed AENA, Ali MY, Abaza SS. The key management of direct/external modulation semiconductor laser response systems for relative intensity noise control. Indones J Electr Eng Comput Sci 2021;21:968–77.
85. Eid MMA, Seliem AS, Rashed ANZ, Mohammed AENA, Ali MY, Abaza SS. Duobinary modulation/predistortion techniques effects on high bit rate radio over fiber systems. Indones J Electr Eng Comput Sci 2021;21: 978–86.
86. Alatwi AM, Rashed ANZ. A pulse amplitude modulation scheme based on in-line semiconductor optical amplifiers (SOAs) for optical soliton systems. Indones J Electr Eng Comput Sci 2021;21:1014–21.
87. Eid MMA, Rashed ANZ, El-Meadawy S, Habib MA. Best selected optical fibers with wavelength multiplexing techniques for minimum bit error rates. J Opt Commun 2020;41:433–43.
88. Alatwi AM, Rashed ANZ, El-Aziz IAA. High speed modulated wavelength division optical fiber transmission systems performance signature. Telkomnika Telecommun Comput Electron Control 2021;19: 380–9.
89. Eid MMA, Rashed ANZ, El-Gammal EM, Delwar TS, Ryu JY. The influence of electrical filters with sequence generators on optical ISL performance evolution with suitable data rates. J Opt Commun 2020; 41:455–70.
90. Alatwi AM, Rashed ANZ, Parvez AHMS, Paul BK, Ahmed K. Beam divergence and operating wavelength bands effects on free space optics communication channels in local access networks. J Opt Commun 2020;41:488–500.
91. Shafkat A, Rashed ANZ, El-Hageen HM, Alatwi AM. The effects of adding different adhesive layers with a microstructure fiber sensor based on surface plasmon resonance: a numerical study. Plasmonics J 2021;16:819–32.
92. Eid MMA, Rashed ANZ. Fiber optic propagation problems and signal bandwidth measurements under high temperature and high dopant germanium ratios. J Opt Commun 2020;41:512–22.
93. Eid MMA, Rashed ANZ. Simulative and analytical methods of bidirectional EDFA amplifiers in optical communication links in the optimum case. J Opt Commun 2020;41:533–50.
94. Eid MMA, Shehata E, Rashed ANZ. Cascaded stages of parametric optical fiber amplifiers with Raman fiber amplifiers for upgrading of telecommunication networks through optical wireless communication channel. J Opt Commun 2020;41:566–76.
95. Eid MMA, Mohammed AENA, Rashed ANZ. Simulative study on the cascaded stages of traveling wave semiconductor optical amplifiers based multiplexing schemes for fiber optic systems improvement. J Opt Commun 2020;41:588–600.
96. Parvin T, Ahmed K, Alatwi AM, Rashed ANZ. Differential optical absorption spectroscopy based refractive index sensor for cancer cell detection. Opt Rev 2021;28:134–43.
97. Eid MMA, Said SM, Rashed ANZ. Gain/noise figure spectra of average power model Raman optical amplifiers in coarse wavelength multiplexed systems. J Opt Commun 2020;41:613–22.
98. Eid MMA, Rashed ANZ, Ahammad MS, Paul BK, Ahmed K. The effects of Tx./Rx. pointing errors on the performance efficiency of local area optical wireless communication networks. J Opt Commun 2020;41: 633–43.
99. Eid MMA, El-Hamid HSA, Rashed ANZ. High-speed fiber system capacity with bidirectional Er-Yb CDFs based on differential phase shift keying (DPSK) modulation technique. J Opt Commun 2020;41:654–66.
100. Eid MMA, Ibrahim A, Rashed ANZ. In line and post erbium-doped fiber amplifiers with ideal dispersion compensation fiber Bragg grating for upgrading optical access networks. J Opt Commun 2020;41:688–700.
101. Eid MMA, Helmy A, Rashed ANZ. Chirped Gaussian pulse propagation with various data rates transmission in the presence of group velocity dispersion (GVD). J Opt Commun 2020;42:13–22.
102. Habib A, Rashed ANZ, El-Hageen HM, Alatwi AM. Extremely sensitive photonic crystal fiber–based cancer cell detector in the terahertz regime. Plasmonics 2021;16:1297–306.
103. Shafkat A, Rashed ANZ, El-Hageen HM, Alatwi AM. Design and analysis of a single elliptical channel photonic crystal fiber sensor for potential malaria detection. J Sol Gel Sci Technol 2022;98:202–11.
104. Eid MMA, Rashed ANZ. Fixed scattering section length with variable scattering section dispersion based optical fibers for polarization

mode dispersion penalties. Indones J Electr Eng Comput Sci 2021;21:1540–7.
105. Eid MMA, Seliem AS, Rashed ANZ, Mohammed AENA, Ali MY, Abaza SS. High sensitivity sapphire FBG temperature sensors for the signal processing of data communications technology. Indones J Electr Eng Comput Sci 2021;21:1567–74.
106. Eid MMA, Seliem AS, Rashed ANZ, Mohammed AENA, Ali MY, Abaza SS. High modulated soliton power propagation interaction with optical fiber and optical wireless communication channels. Indones J Electr Eng Comput Sci 2021;21:1575–83.
107. Eid MMA, Rashed ANZ, Delwar TS, Siddique A, Ryu JY. Linear/cubic measured pulse numerically with electrical jitter amplitude variations for the impact on fiber communication systems. J Opt Commun 2021;42:33–43.
108. Eid MMA, El-Meadawy S, Mohammed AENA, Rashed ANZ. Wavelength division multiplexing developed with optimum length-based EDFA in the presence of dispersion-compensated fiber system. J Opt Commun 2021;42:55–70.
109. Eid MMA, Sorathiya V, Lavadiya S, Habib MA, Helmy A, Rashed ANZ. Dispersion compensation FBG with optical quadrature phase shift keying (OQPSK) modulation scheme for high system capacity. J Opt Commun 2021;42:86–100.
110. Eid MMA, Sorathiya V, Lavadiya S, Shehata E, Rashed ANZ. Free space and wired optics communication systems performance improvement for short-range applications with the signal power optimization. J Opt Commun 2021;42:114–22.
111. Eid MMA, Rashed ANZ. Numerical simulation of long-period grating sensors (LPGS) transmission spectrum behavior under strain and temperature effects. Sens Rev J 2021;41:192–9.
112. Eid MMA, Rashed ANZ. Basic FBG apodization functions effects on the filtered optical acoustic signal. Indones J Electr Eng Comput Sci 2021;22:287–96.
113. Eid MMA, El-Meadawy S, Mohammed AENA, Rashed ANZ. High data rates in optic fiber systems based on the gain optimization techniques. J Opt Commun 2021;42:130–44.
114. Ahmed K, AlZain MA, Abdullah H, Luo Y, Vigneswaran D, Faragallah OS, et al. Highly sensitive twin resonance coupling refractive index sensor based on gold- and MgF2-coated nano metal films. Biosensors 2021;11:104–13.
115. Delwar TS, Siddique A, Ranjan Biswal M, Rashed ANZ, Jee AJ, Ryu Y. Novel multi-user MC-CSK modulation technique in visible light communication. Opt Quant Electron 2021;53:196–206.
116. Eid MMA, Habib MA, Anower MS, Rashed ANZ. Hollow core photonic crystal fiber (PCF)–Based optical sensor for blood component detection in terahertz spectrum. Braz J Phys 2021;51:1017–25.
117. Eid MMA, Sorathiya V, Lavadiya S, El-Hamid HSA, Rashed ANZ. Wide band fiber systems and long transmission applications based on optimum optical fiber amplifiers lengths. J Opt Commun 2021;42:155–70.
118. Eid MMA, Sorathiya V, Lavadiya S, Shehata E, Rashed ANZ. Optical switches based semiconductor optical amplifiers (SOAs) for performance characteristics enhancement by using various electrical pulse generators. J Opt Commun 2021;42:183–95.
119. Eid MMA, Rashed ANZ, Sorathiya V, Lavadiya S, Habib MA, Amiri IS. GaAs electro-optic absorption modulators performance evaluation, under high-temperature variations. J Opt Commun 2021;42:200–13.
120. Abdullaha H, Ahmed K, Alama MS, Rashed ANZ, Mitua SA, Al-Zahranid FA, et al. High sensitivity refractive index sensor based on triple layer MgF2-gold-MgF2 coated nano metal films photonic crystal fiber. Optik – Int J Light Electron Opt 2021;241:166–76.
121. Eid MMA, Sorathiya V, Lavadiya S, El-Aziz IAA, Rashed ANZ. Free space optics communication channel with amplitude/frequency shift keying modulation technique based raised cosine line coding. J Opt Commun 2021;42:225–36.
122. Eid MMA, Rashed ANZ, Rajagopal M, Parimanam J, Abhay V. Integrated role between VCSEL diodes and Gaussian pulse generators with ideal EDFA for self phase modulation instability management. J Opt Commun 2021;42:255–70.
123. Eid MMA, Sorathiya V, Lavadiya S, Helmy A, Rashed ANZ. Technical specifications and spectral performance characteristics of dispersion flattened fiber (DFF) in optical fiber systems. J Opt Commun 2021;42:280–95.
124. Eid MMA, Rashed ANZ. Hybrid NRZ/RZ line coding scheme based hybrid FSO/FO dual channel communication systems. Indones J Electr Eng Comput Sci 2021;22:866–73.
125. Bulbul AAM, Rashed ANZ, El-Hageen HM, Alatwi AM. Design and numerical analysis of an extremely sensitive PCF-based sensor for detecting kerosene adulteration in petrol and diesel. Alex Eng J 2021;60:5419–30.
126. Eid MMA, Sorathiya V, Lavadiya S, El-Aziz IAA, Asaduzzaman S, Rehana H, et al. ROF systems performance efficiency based on continuous phase frequency shift keying phase modulation scheme. J Opt Commun 2021;42:305–13.
127. Habib MA, Anower MS, AlGhamdi A, Faragallah OS, Eid MMA, Rashed ANZ. Efficient way for detection of alcohols using hollow core photonic crystal fiber sensor. Opt Rev 2021;28:383–92.
128. Eid MMA, Sorathiya V, Lavadiya S, Parmar J, Patel SK, Ali SA, et al. CWDM communication system based inline erbium-doped fiber amplifiers with the linear geometrical polarization model. J Opt Commun 2021;42:320–33.
129. Sorathiya V, Lavadiya S, AlGhamdi A, Faragallah OS, El-sayed HS, Eid MMA, et al. A comparative study of broadband solar absorbers with different gold metasurfaces and MgF2 on tungsten substrates. J Comput Electron 2021;20:1840–50.
130. Lavadiya SP, Sorathiya V, Kanzariya S, Chavda B, Faragallah OS, Eid MMA, et al. Design and verification of novel low profile miniaturized pattern and frequency tunable microstrip patch antenna using two PIN diodes. Braz J Phys 2021;51:1303–13.
131. Eid MMA, Urooj S, Alwadai NM, Rashed ANZ. AlGaInP optical source integrated with fiber links and silicon avalanche photo detectors in fiber optic systems. Indones J Electr Eng Comput Sci 2021;23:847–54.
132. Urooj S, Alwadai NM, Ibrahim A, Rashed ANZ. Simulative study of raised cosine impulse function with Hamming grating profile based Chirp Bragg grating fiber. J Opt Commun 2021;42:350–65.
133. Jibon RH, Bulbul AAM, Nahid AA, Faragallah OS, Baz M, Eid MMA, et al. Design and numerical analysis of a photonic crystal fiber (PCF)-based flattened dispersion THz waveguide. Opt Rev 2021;28:564–72.
134. Eid MMA, Mohammed AENA, Rashed ANZ. Different soliton pulse order effects on the fiber communication systems performance evaluation. Indones J Electr Eng Comput Sci 2021;23:1485–92.
135. Urooj S, Alwadai NM, Sorathiya V, Lavadiya S, Parmar J, Patel SK, et al. Differential coding scheme based FSO channel for optical coherent DP-16 QAM transceiver systems. J Opt Commun 2021;42:377–90.
136. Rashed ANZ, Zaky WF, Eid MMA, Faragallah OS. Dynamic response based on non-linear material for electrical and optical analogy of full optical oscillator. Opt Quant Electron 2021;53:234–50.
137. Rashed ANZ, Zaky WF, El-Hageen HM, Alatwi AM. Technical specifications for an all-optical switch for information storage and processing systems. Eur Phys J Plus 2021;136:1100–12.

138. Sorathiya V, Lavadiya S, Parmar B, Das S, Krishna M, Faragallah OS, et al. Numerical investigation of the tunable polarizer using gold array and graphene metamaterial structure for an infrared frequency range. Appl Phys B 2022;128:555–70.
139. Delwar TS, Siddique A, Biswal MR, Behera P, Rashed ANZ, Choi Y, et al. A novel dual mode configurable and tunable high-gain, high-efficient CMOS power amplifier for 5G applications. Integrat VLSI J 2022;83: 77–87.
140. Eid MMA, Arunachalam R, Sorathiya V, Lavadiya S, Patel SK, Parmar J, et al. QAM receiver based on light amplifiers measured with effective role of optical coherent duobinary transmitter. J Opt Commun 2022; 43:20–33.
141. Sorathiya V, Lavadiya S, AlGhamdi A, Faragallah OS, El-Sayed HS, Parmar B, et al. Hilbert resonator based multiband tunable graphene metasurface polarizer for lower THz frequency. J Comput Electron 2022;21:280–8.
142. Mohammad A, Alzaidi MS, Eid MMA, Sorathiya V, Lavadiya S, Patel SK, et al. First order surface grating fiber coupler under the period chirp and apodization functions variations effects. Indones J Electr Eng Comput Sci 2022;25:1020–9.
143. Mohammad A, Alzaidi MS, Eid MMA, Sorathiya V, Lavadiya S, Patel SK, et al. Free space optical communication system for indoor applications based on printed circuit board design. Indones J Electr Eng Comput Sci 2022;25:1030–7.
144. Sorathiya V, Lavadiya S, Parmar BS, Baxi S, Dhankot T, Faragallah OS, et al. Tunable squared patch based graphene metasurface infrared polarizer. Appl Phys B 2022;128:247–60.
145. Lavadiya S, Sorathiya V, Faragallah OS, El-Sayed HS, Eid MMA, Rashed ANZ. Infrared graphene assisted multi-band tunable absorber. Opt Quant Electron 2022;54:145–65.
146. Jibon RH, Ahmed M, Abd-Elnaby M, Rashed ANZ, Eid MMA. Design mechanism and performance evaluation of photonic crystal fiber (PCF) based sensor in the THz regime for sensing noxious chemical substrates of poultry feed. Appl Phys A 2022;128:1656–66.
147. Sorathiya V, Lavadiya S, Thomas L, Abd-Elnaby M, Rashed ANZ, Eid MMA. Graphene based tunable short band absorber for infrared wavelength. Appl Phys B 2022;128:101–16.
148. Dutta N, Patel SK, Faragallah OS, Baz M, Rashed ANZ. Caching scheme for information-centric networks with balanced content distribution. Int J Commun Syst 2022;35:16–29.
149. Lavadiya SP, Sorathiya V, Kanzariya S, Chavda B, Naweed A, Faragallah OS, et al. Low profile multiband microstrip patch antenna with frequency reconfigurable feature using PIN diode for S,C, X, and Ku band applications. Int J Commun Syst 2022;35:30–5.
150. Asaduzzaman S, Rehana H, Aziz T, Faragallah OS, Baz M, Eid MMA, et al. Key performance parameters estimation with Epsilon near zero (ENZ) for Kagome photonic crystal fiber in THz system. Opt Quant Electron 2022;54:1234–55.
151. Patel SK, Solanki N, Charola S, Parmar J, Zakaria R, Faragallah OS, et al. Graphene based highly sensitive refractive index sensor using double split ring resonator metasurface. Opt Quant Electron 2022; 54:20–33.
152. Sorathiya V, Lavadiya S, Faragallah OS, Eid MMA, Rashed ANZ. D shaped dual core photonics crystal based refractive index sensor using graphene–titanium–silver materials for infrared frequency spectrum. Opt Quant Electron 2022;54:1123–34.
153. Hossain E, Hossain MS, Hossain MS, Jannat SA, Huda M, Alsharif S, et al. Brain tumor auto-segmentation on multimodal imaging modalities using deep neural network. Comput Mater Continua 2022; 72:4509–23.